Functional connectivity of white matter as a biomarker of cognitive decline in Alzheimer's disease

*Yurui Gao[1,2], Anirban Sengupta[1,3], Muwei Li[1,3], Zhongliang Zu[1,3], Baxter P. Rogers[1,3], Adam W. Anderson[1,2,3], Zhaohua Ding[1,4], John C. Gore[1,2,3], for the Alzheimer's Disease Neuroimaging Initiative[a]

[1]Institute of Imaging Science, Vanderbilt University Medical Center, Nashville, TN, 37232, USA

[2]Biomedical Engineering, Vanderbilt University, Nashville, TN, 37212, USA

[3]Radiology and Radiological Sciences, Vanderbilt University Medical Center, Nashville, TN, 37232, USA

[4]Electrical Engineering and Computer Science, Vanderbilt University, Nashville, TN, 37212, USA

* Corresponding author: Yurui Gao, PhD, Department of Biomedical Engineering, Vanderbilt University, Nashville, TN, 37235, USA (yurui.gao@vanderbilt.edu)

[a] Data used in preparation of this article were obtained from the Alzheimer's Disease Neuroimaging Initiative (ADNI) database (adni.loni.usc.edu). As such, the investigators within the ADNI contributed to the design and implementation of ADNI and/or provided data but did not participate in analysis or writing of this report. A complete listing of ADNI investigators can be found at: http://adni.loni.usc.edu/wp-content/uploads/how_to_apply/ADNI_Acknowledgement_List.pdf

Abstract

Objective: *In vivo* functional changes in white matter during the progression of Alzheimer's disease (AD) have not been previously reported. Our objectives are to measure changes in white matter functional connectivity (FC) in an aging population undergoing cognitive decline as AD develops, to establish their relationship to neuropsychological scores of cognitive abilities, and to assess their performance as predictors of AD.

Methods: Analyses were conducted using resting state functional MRI (rsfMRI) and neuropsychological data from 383 ADNI participants, including 136 cognitive normal (CN) controls, 46 with significant memory concern, 83 with early mild cognitive impairment (MCI), 37 with MCI, 46 with late MCI, and 35 with AD dementia. We used novel analyses of whole brain rsfMRI data to derive FC metrics between white matter tracts and discrete cortical volumes, as well as FC metrics between different white matter tracts, and their relationship to 6 cognitive measures. We then implemented supervised machine learning on white matter FCs to classify the participants and evaluated the performance.

Results: Significant decreases were found in white matter FCs with prominent, specific, regional deficits appearing in late MCI and AD dementia patients relative to CN. These changes significantly correlated with behavioral measurements of impairments in cognition and memory. The sensitivity and specificity for distinguishing AD dementia and CN using white matter FCs were 0.83 and 0.81 respectively.

Conclusions and Relevance: The white matter FC decreased in late MCI and AD dementia patients compared to CN participants, and the white matter FC correlates with cognitive measures. White matter FC based classification shows promise for differentiating AD patients from CN. It is suggested that white matter FC may be a novel imaging biomarker of AD progression.

Key words: White matter, functional connectivity, Alzheimer's disease, cognitive decline, fMRI, machine learning

Introduction

Alzheimer's disease (AD) is the most common progressive neurodegenerative disorder, which begins at a pre-symptomatic stage before subjects exhibit increasingly severe cognitive impairments and ultimately, dementia [1, 2]. Histopathological evidence of degeneration during this progression has been observed in human brains in both gray matter (GM) and white matter (WM) [3, 4]. While there has been considerable emphasis on cortical changes, pathological alterations of WM post mortem have also been reported not only in late stages of AD (associated with loss of axons and oligodendrocytes [5] and concomitant with vascular abnormalities [6, 7]), but also in earlier, pre-clinical stages, probably related to amyloid toxicity [8]. Moreover, tissue shrinkage has been found to be even more prominent in WM than in GM in early stage disease [3]. Potentially, therefore, appropriate measures of changes within WM may be valuable biomarkers of neurodegeneration in AD. However, to date there have been no studies of functional changes in WM in AD, and there remain no imaging metrics from any modality that reliably reflect behavioral or cognitive changes in the progression towards AD.

Functional magnetic resonance imaging (fMRI) has been previously used to detect functional alterations arising in AD [9-11] but to date such studies have been almost exclusively focused on GM, with very limited exceptions [12, 13]. FMRI detects changes in MRI images caused by variations in blood volume and/or oxygenation (blood oxygenation level dependent (BOLD) effects) that in cortex correspond to changes in neural activity. Correlations across time between fluctuations in MRI signals from different cortical regions in a resting state are interpreted as indicators of functional connectivity (FC) between them. BOLD signals are expected to be much smaller in WM than in GM and are usually excluded from image analyses. However, recently we demonstrated that BOLD fluctuations in WM share common features with those from GM and they correlate significantly with BOLD signals from specific cortical regions to which they connect [14, 15]. Relationships between WM tracts and GM regions may be summarized by a functional correlation matrix (FCM) of their pair-wise correlations at rest, while different WM tracts can be inter-related using a similar approach.

In this study, we extended these new findings and analyses, originally described in reference [14, 16], to quantify changes in WM fMRI metrics during the progression to AD. We measured the differences in the FCMs for WM-GM correlations (FCM_{WG}) and WM-WM (FCM_{WW}) between a healthy group and each of five participant groups at different stages of cognitive impairments. We also subsequently evaluated the correlations between these FC metrics and behavioral measures of cognition and memory. Finally, we explored the use of machine learning to

differentiate between the controls and patients at different AD stages to evaluate how well WM FC alone can classify subjects.

Materials and Methods

Data used in this study were all obtained from the database of the Alzheimer's Disease Neuroimaging Initiative (ADNI) (adni.loni.usc.edu).

Participants

The participant selection criteria were that 1) baseline rsfMRI images were available in ADNI-2 or ADNI-3 (if the participant was available in both ADNI-2 and ADNI-3, then data in ADNI-3 were selected); 2) participants were aged 60-90 years; 3) multi-band rsfMRI acquisitions were excluded and 4) the data survived MRI processing.

The participants were grouped as cognitive normal (CN), significant memory concerns (SMC), early mild cognitive impairments (EMCI), mild cognitive impairments (MCI), late MCI (LMCI) and AD dementia (ADD). The full criteria for clinical classifications are described in the ADNI manual [17].

MRI

3T rsfMRI and T1-weighted (T1w) data, acquired at multiple institutions with the same imaging protocol, were preprocessed using the toolbox DPARSFA [18]. First, the rsfMRI images were corrected for slice timing and head motion. Twenty-four motion parameters [19] and mean CSF signal were regressed out. The resulting rsfMRI data were filtered (passband=0.01-0.1Hz), coregistered to a common space [20], detrended, and then normalized voxel-wise into a time-course with zero mean and unit variance. Next, WM, GM, and cerebrospinal fluid (CSF) were segmented using the T1w images [21] and their tissue probability maps were normalized to the common space.

Calculation of Functional Correlation Matrix (FCM)

The calculations of correlations for each participant were restricted to WM and GM regions of interest (ROIs, listed in **Table 1**) that were defined by the Eve atlas [22] (48 WM tracts, see **S1 Fig** in Supplement) and PickAtlas [23] (82 Brodmann areas) and were further constrained within masks generated by thresholding the WM and GM probability maps at 0.8. The preprocessed time-courses were averaged over the voxels within each ROI and for each pair of WM and GM ROIs they were then cross correlated, excluding any time points with large motions (framewise displacement [24] >0.5). The resulting 48x82 correlation coefficients formed an FCM of WM-GM pairs (FCM_{WG}). Similarly, the mean time-courses for each pair of WM ROIs were cross correlated and the 48x48 correlation

coefficients formed an FCM of WM-WM pairs (FCM_{WW}). Meanwhile, we generated FCM of GM-GM pairs (FCM_{GG}) to confirm the validity of our processing pipeline. The possible influences of age, gender, years of education and acquisition-site were regressed out from FCM using a generalized linear model.

Table 1. List of WM and GM ROIs

White Matter (WM) ROIs	**Gray Matter (GM) ROIs**
CST: Corticospinal Tract	BA1: Primary Somatosensory Cortex 1
ML: Medial Lemniscus	BA2: Primary Somatosensory Cortex 2
ICP: Inferior Cerebellar Peduncle	BA3: Primary Somatosensory Cortex 3
SCP: Superior Cerebellar Peduncle	BA4: Primary Motor Cortex
CP: Cerebral Peduncle	BA5: Somatosensory Association Cortex
ALIC: Anterior Limb of Internal Capsule	BA6: Premotor and Supplementary Motor
PLIC: Posterior Limb of Internal Capsule	BA7: Visuo-Motor Coordination
RLIC: Retrolenticular Limb of Internal Capsule	BA8: Frontal Eye Fields
ACR: Anterior Corona Radiata	BA9: Dorsolateral Prefrontal Cortex
SCR: Superior Corona Radiata	BA10: Anterior Prefrontal Cortex
PCR: Posterior Corona Radiata	BA11: Orbitofrontal Area
PTR: Posterior Thalamic Radiation (include OR)	BA13: Insular Cortex
SS: Sagittal Stratum (include inferior longitudinal fasciculus and fronto-occipital fasciculus)	BA17: Primary Visual Cortex (V1)
EC: External Capsule	BA18: Secondary Visual Cortex (V2)
CGG: Cingulum (Cingulate Gyrus)	BA19: Associative Visual Cortex (V3-5)
CGH: Cingulum (Hippocampus)	BA20: Inferior Temporal Gyrus
FXC: Fornix (Cres)	BA21: Middle Temporal Gyrus
SLF: Superior Longitudinal Fasciculus	BA22: Superior Temporal Gyrus
SFO: Superior Fronto-Occipital Fasciculus	BA23: Ventral Posterior Cingulate Cortex
UF: Uncinate Fasciculus	BA24: Ventral Anterior Cingulate Cortex
TAP: Tapetum	BA25: Subgenual Area
MCP: Middle Cerebellar Peduncle	BA26: Ectosplenial Portion of Retrosplenial Region
PCT: Pontine Crossing Tract	BA27: Piriform Cortex
GCC: Genu of Corpus Callosum	BA28: Ventral Entorhinal Cortex
BCC: Body of Corpus Callosum	BA29: Retrosplenial Cingulate Cortex
SCC: Splenium of Corpus Callosum	BA30: Part of Cingulate Cortex
FX: Fornix	BA32: Dorsal Anterior Cingulate Cortex
	BA34: Dorsal Entorhinal Cortex
	BA35: Perirhinal Cortex
	BA36: Ectorhinal Area
	BA37: Occipitotemporal Area (part of fusiform gyrus and interior temporal gyrus
	BA38: Temporopolar Area
	BA39: Angular Gyrus
	BA40: Supramarginal Gyrus
	BA41: Auditory Cortex 1
	BA42: Auditory Cortex 2
	BA43: Primary Gustatory Cortex
	BA44: Pars Opercularis
	BA45: Pars Triangularis
	BA46: Dorsolateral Prefrontal Cortex
	BA47: Pars Orbitalis

Neuropsychological Testing

Neuropsychological scores included the scores of the Mini-Mental State Examination (MMSE), Clinical Dementia Rating (CDR) global, CDR sum of boxes (CDR-SOB), Global Deterioration Scale (GDS), functional assessment questionnaire (FAQ) total, Wechsler memory scale-logical memory II subscale (WMS-LMII), Alzheimer's Disease Assessment Scale-Cognitive (ADAS-Cog) and Hachinski scale, which are the most commonly used for clinical assessment and AD studies.

Statistical Analysis

The characteristics of the six subject groups were summarized, and the differences among groups were tested by one-way ANOVA or chi-squared test.

The FCMs within each clinical group were averaged to produce a mean matrix (mFCM). Differences in the mFCM values, and the effect sizes of these differences [25] between the CN group and every other group were calculated. Permutation tests (10,000 permutations) were conducted for each FCM element across all participants within any two comparison groups. The resulting *P*-values were corrected for multiple comparisons using a false discovery rate [26], denoted as P_{FDR}. To estimate the overall connectivity of each WM tract, the FCM elements corresponding to each WM ROI were averaged. The mean and standard deviation of each WM-tract-wise FC across participants within each group were then calculated. The WM-tract-wise FC in the CN group were compared with every other group using unpaired-sample *t*-tests.

To measure the general trend of WM related functional connectivity as disease progresses, all the elements of each mFCM were averaged, providing a metric of overall-connectivity for each participant, and then the group mean and standard deviation of the overall-connectivity for each subject group were estimated and finally normalized by linear scaling.

The associations between each single FCM element and neuropsychological scores were evaluated by calculating the linear correlation coefficients between the element and each score across all participants. To gauge the overall correlation of a WM tract's connectivity with the score, significant correlation coefficients along the same WM tract were summed.

To further evaluate the associations between combined FCM elements and each neuropsychological score, a random forest (RF) regression model was trained to predict the score after feature selection from all FCM elements.

The value of goodness of fit, R^2 was calculated based on comparing true and predicted scores.

Machine Learning Classification

A support vector machine (SVM) with a radial-basis function kernel was used to classify the CN group and different combinations of groups of impaired subjects (i.e., ADD alone; LMCI and ADD together; MCI, LMCI and ADD together; EMCI, MCI, LMCI and ADD together; and SMC, EMCI, MCI, LMCI and ADD together). We used all FCM_{WG} and FCM_{WW} elements as initial features and implemented an RF algorithm to select those features that provided more accurate classifications [27]. In detail, the number of trees for the RF classifier was chosen to be 200 as it was observed that increasing the number of trees further resulted in no significant reduction of classification error. The splitting criterion for RF was based on the GUIDE algorithm [28]. Individual feature importance was computed by measuring how much the predictive accuracy of the RF classifier deteriorated when the feature's values were randomly permuted [2]. The idea is that altering the value of an important feature will degrade the performance of a classifier. After obtaining the importance of each feature individually, the features that did not improve performance at all were at first removed from the set. The remaining features were arranged in descending order of their importance. Features were added sequentially, and classification error was noted for this cumulative feature set. The optimal feature set was taken to be the one, which provided the lowest classification error. A similar method was used for feature selection in the case of regression analysis abovementioned. There were 5064 WM functional connectivities in this study, so the features, which were arranged in descending order of importance, were added five at a time sequentially to reduce the computational load. In the case of the classification task, SVM with a radial-basis function (RBF) kernel was optimized with respect to C and Gamma, the two hyper-parameters. C regularized the classifier, and Gamma denoted variance of the RBF kernel and controlled the width of the kernel. Mean squared error of a 10-fold cross-validation (CV) was calculated to measure the classification error. More specifically, the data were split into 10 subsets. The SVM model was trained on 9 subsets and then evaluated on the remaining subsets. This process was repeated 10 times, with a different subset as testing data each time. One error was estimated at each time and the final error was the average of the 10 errors. Also, the penalty involved for misclassification of the disease group versus control group was manually varied so that data imbalance between the groups did not tilt the model accuracy towards one group [29]. Moreover, the receiver-operating characteristic (ROC) analysis was performed and the area under curve (AUC), sensitivity, and specificity were noted.

Subjects that did not have any behavioral scores were removed from the regression study.

Results

Participant characteristics

Table 2 shows characteristics of all 383 participants, grouped into CN (n=136), SMC (n=46), EMCI (n=83), MCI (n=37), LMCI (n=46) and ADD (n=35), in order of disease severity. Among these groups, no significant differences in age (P=0.93), sex (P=0.22), handedness (P=0.99), years of education (P=0.23), brain volume (P =0.41) or Hachinski scale (P =0.25) were observed. The scanner vendor breakdown, CSF amyloid beta, CSF Tau, CSF p-tau, FDG-PET, MMSE, CDR global, CDR-SOB, GDS, FAQ, WMS-LMII and ADAS-Cog scores did differ significantly among groups (P <0.007).

Table 2. Baseline Participant Characteristics.

Characteristics	CN (n=136)	SMC (n=46)	EMCI (n=83)	MCI (n=37)	LMCI (n=46)	ADD (n=35)	*P*-value (ANOVA or chi-square)
Age, mean (SD), y	74.5 (7.1)	75.3 (5.8)	74.5 (7.0)	74.3 (7.2)	74.6 (6.8)	75.6 (6.8)	0.93
Female sex, No. (%)	82(60)	26(57)	42 (51)	15 (41)	21 (46)	16 (46)	0.22
Handedness, No. (%)	126 (92)	42 (91)	76 (92)	34 (92)	42 (91)	33 (94)	0.99
Education, mean (SD), y	16.8 (2.3)	16.8 (2.6)	16.0 (2.7)	16.3 (2.5)	16.4 (2.9)	16.2 (2.7)	0.23
Scanner vendor (S:G:P)	86:27:24	18:15:13	31:11:41	18:9:10	19:6:21	6:3:26	<0.001
Brain volume (SD) $X10^5$	10.6 (0.9)	10.7 (0.9)	10.6 (2.2)	10.4 (1.0)	10.4 (1.1)	10.2 (1.2)	0.41
CSF Amyloid beta (SD) $X10^2$	13.5 (4.3)	13.8 (3.3)	11.6 (4.6)	11.4 (2.5)	10.5 (4.0)	6.7 (2.8)	<0.001
CSF Tau	261 (104)	223 (78)	273 (139)	237 (113)	275 (132)	355 (130)	0.007
CSF p-Tau	23.9 (10.6)	19.9 (8.1)	25.7 (15.5)	23.2 (12.1)	26.3 (14.3)	34.6 (13.3)	0.004
FDG-PET	1.34 (0.09)	1.34 (0.09)	1.30 (0.10)	1.28 (0.13)	1.26 (0.12)	1.09 (0.14)	<0.001
MMSE score, mean (SD)	29.1 (1.7)	29.1 (1.0)	27.4 (2.9)	28.0 (1.5)	25.8 (5.6)	22.4 (3.2)	<0.001
CDR global score, mean (SD)	0.0 (0.2)	0.1 (0.2)	0.4 (0.3)	0.5 (0.0)	0.6 (0.5)	0.8 (0.2)	<0.001
CDR-SOB score, mean (SD)	0.3 (1.0)	0.1 (0.4)	1.7 (2.2)	1.2 (0.8)	2.6 (3.2)	4.7 (1.5)	<0.001
GDS score, mean (SD)	0.8 (1.5)	1.3 (1.3)	1.8 (2.0)	1.5 (1.3)	1.8 (2.3)	1.5 (1.3)	<0.001
FAQ score, mean (SD)	1.0 (3.7)	0.4 (0.8)	4.2 (6.5)	3.1 (4.4)	6.5 (8.7)	14.6 (6.2)	<0.001
WMS-LMII score, mean (SD)	15.4 (3.3)	15.4 (3.0)	12.4 (5.1)	9.2 (3.8)	9.7 (5.0)	4.5 (3.1)	<0.001
ADAS-Cog score, mean (SD)	9.6 (4.4)	8.2 (3.1)	12.0 (6.0)	12.3 (3.4)	14.0 (8.3)	22.7 (7.4)	<0.001
Hachinski scale, mean (SD)	0.5 (0.7)	0.6 (1.0)	1.0 (1.2)	0.8 (1.2)	0.7 (0.9)	0.9 (0.9)	0.25

Note: S=Siemens; G=GE Medical Systems; P=Philips Medical System and Philips Healthcare. FDG-PET: average FDG-PET of angular, temporal, and posterior cingulate.

WM functional connectivity at baseline

Fig 1ac shows the mean FCM_{WG} ($mFCM_{WG}$) and mean FCM_{WW} ($mFCM_{WW}$) for each clinical group. The overall patterns of $mFCM_{WG}$ or $mFCM_{WW}$ appear similar across the six groups. The mean correlation coefficient of each WM tract across GM ROIs or WM ROIs is illustrated in **Fig 1bd**, showing that cingulum (cingulate gyrus) (CGG), external capsule (EC) and internal capsule (IC) have higher correlations averaged over GM ROIs, and IC, splenium of corpus callosum (SCC), superior longitudinal fasciculus (SLF), and middle cerebellar peduncle (MCP) have

higher WM-averaged correlations.

Comparisons between $mFCM_{WW}$ (**Fig 1c**) and the group mean of GM-GM FCM ($mFCM_{GG}$, **S2 Fig** in Supplement) shows a generally lower level of WM-WM correlation, with a relative decrease of 25-30% in overall average of FCM for every study group.

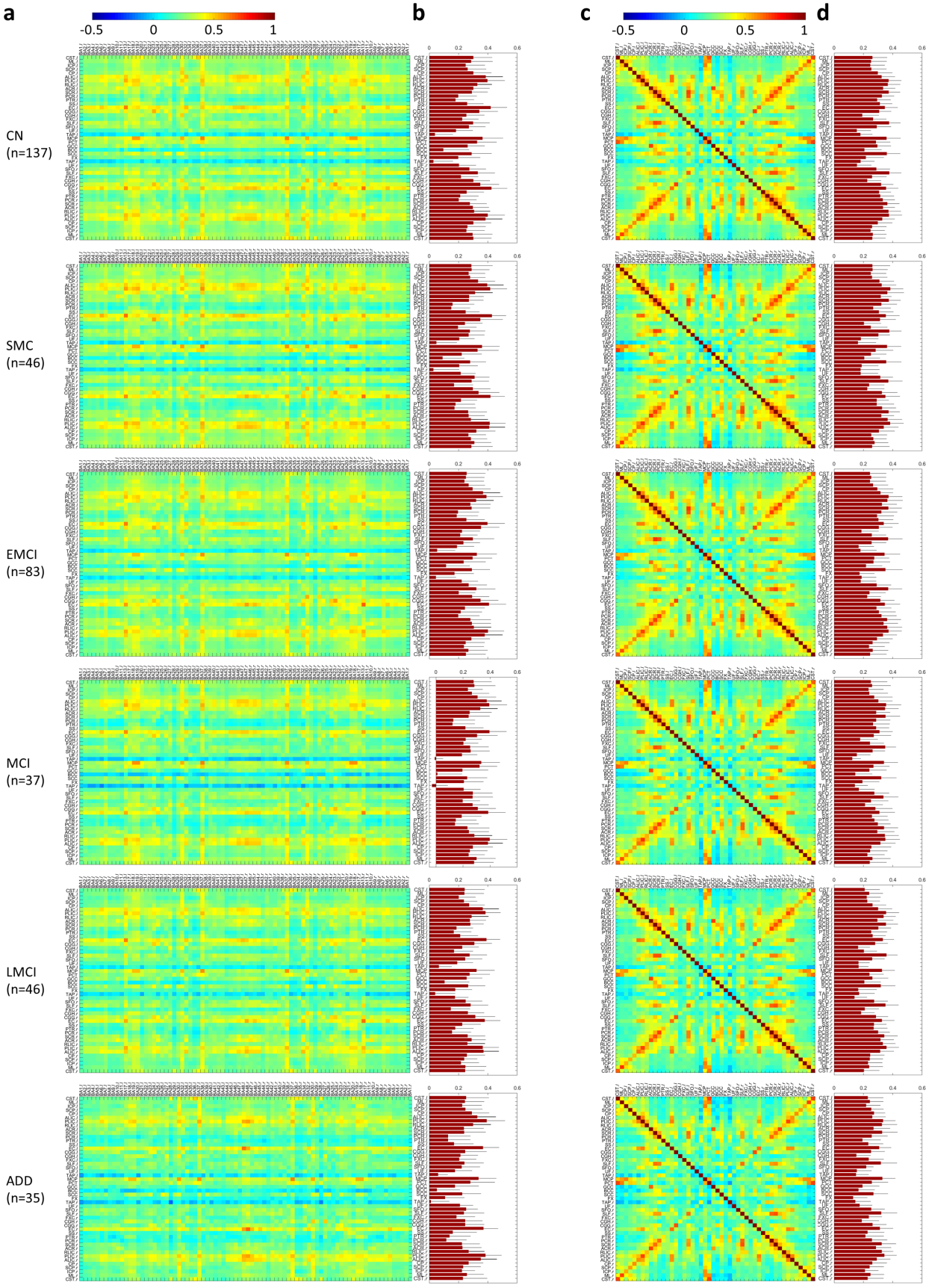

Fig 1. Mean of WM-GM and WM-WM functional correlation matrices ($mFCM_{WG}$ and $mFCM_{WW}$) as well as GM-averaged and WM-averaged correlation coefficients of WM tracts for each group were analyzed. Mean of FCM_{WG} (A) or FCM_{WW} (C) across all participants within group of CN, SMC, EMCI, MCI, LMCI or ADD. Each element in $mFCM_{WG}$ (or $mFCM_{WW}$) is the group mean correlation coefficient of the averaged BOLD time-courses between one WM region and one GM (or WM) region. GM-averaged (B) and WM-averaged (D) correlation coefficients of WM tracts for each group. Group mean (red bar) and standard deviation (black error bar) for each WM tract are shown. Full names of WM ROIs and GM ROIs are listed in **Table 1**.

WM functional connectivity deficits in progression to AD

In LMCI or ADD patients, significant FC decreases were observed in a number of WM-GM pairs (**Fig 2a, f**) and WM-WM pairs (upper triangle in **Fig 2d, i**) compared with CN participants (P_{FDR}<0.05) and there are obvious horizontal patterns in the difference matrices, corresponding to specific WM tracts. In particular, the corpus callosum (CC, including GCC, BCC and SCC), SLF_{lr}, CGG_{lr}, sagittal stratum (SS_{lr}), posterior thalamic radiation (PTR_{lr}) and corona radiata (CR_{lr}, including ACR, SCR and PCR) show profound declines in WM-GM connectivity in the ADD groups relative to the CN group (**Fig 2g**), consistent with previous findings showing microstructural degeneration detected by diffusion MRI in CC, SLF, CGG, SS, PTR and CR in ADD patients[30]. The SS_{lr}, fornix (cres) (FXC_{lr}), SLF_{lr}, right hippocampal cingulum (CGH_r), EC_r, PTR_r and PCR_r show significant decreases in WM-GM connectivity in the LMCI group relative to CN group (**Fig 2b**). The CC, SLF_{lr}, CGH_{lr}, CGG_{lr}, EC_r, SS_{lr}, PTR_{lr}, PCR_{lr}, SCR_{lr}, ACR_l, $RLIC_{lr}$ and $PLIC_{lr}$ show significant declines in inter-tract FC in both the LMCI and ADD groups relative to the CN group (**Fig 2e, j**). Moreover, the effect sizes of group deficits with P_{FDR}<0.05 were mostly larger than 0.3 (**Fig 2c, h** and lower triangle in **Fig 2d, i**).

By contrast, no significant changes in FCM_{WG} or FCM_{WW} between CN and any of the early disease groups (i.e., SMC, EMCI and MCI) were observed at the same *P*-value threshold. But their mean P_{FDR} were 0.99, 0.65, and 0.22, respectively, suggesting a progression towards significant differences. By contrast, previous studies on brain microstructure reported alterations in a few selected WM regions in MCI participants, involving cingulate bundle, inferior FOF and parahippocampal subgyral fibers [31, 32], where connectivity deficits were found in our LMCI and ADD cases.

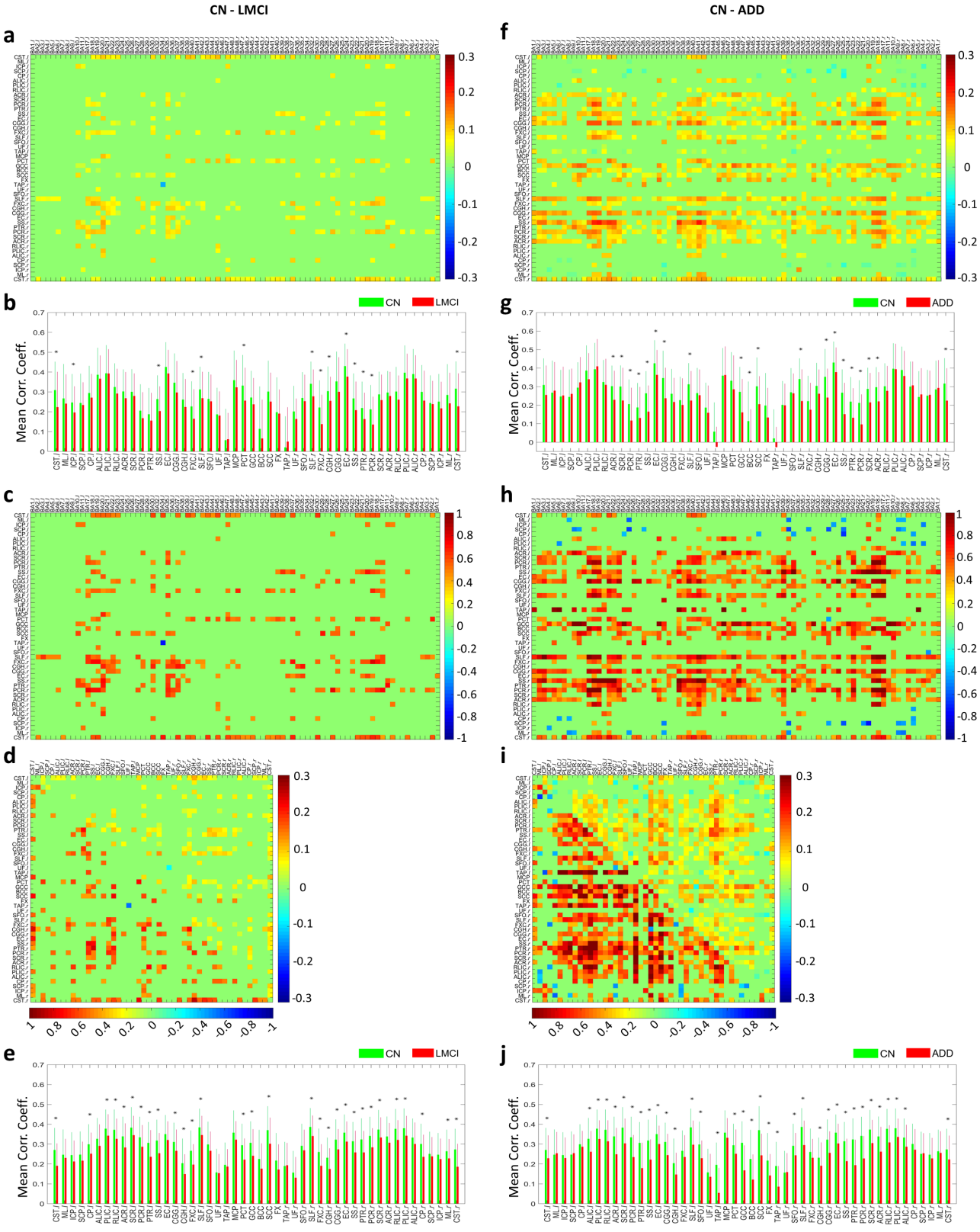

Fig 2. Significant differences of $mFCM_{WG}$ and $mFCM_{WW}$ between controls and impaired groups. (**a, f**) Difference of subtracting $mFCM_{WG}$ of LMCI (**a**) or ADD (**f**) from $mFCM_{WG}$ of CN group. The *P*-value for each element was derived from permutation-test (10,000 permutations) across all participants within groups, and then adjusted using an FDR. Those elements with P_{FDR} >0.05 were set to be zero. (**b, g**) GM-averaged correlation coefficients of WM tracts in CN group (green) and LMCI group (red) (**b**) and in CN group (green) and ADD group (red) (**g**). Mean and standard deviation for each WM tract are shown, and black asterisks (*) denote p <0.05 calculated by unpaired-sample t-test of mean correlation coefficients. (**c, h**) Effect size of the $mFCM_{WG}$ difference between CN and LMCI (**c**) or ADD (**h**), thresholded by P_{FDR}. (**d, i**) Difference of $mFCM_{WW}$ between CN and LMCI or ADD (upper triangle) and effect size of the $mFCM_{WW}$ difference (lower triangle). (**e, j**) WM-averaged correlation coefficients of WM tracts in CN group (green) and LMCI group (red) (**e**) and in CN group (green) and ADD group (red) (**g**).

Correlation between WM functional connectivity and neuropsychological scores

The normalized group means of overall-connectivity decreased gradually until the MCI stage, and then fell rapidly to very low values as MCI progressed to LMCI and ADD stages (**Fig 3a**), a behavior which conforms to current hypothetical models of AD evolution [33]. The corresponding normalized overall trends in 7 behavioral measures across groups (**Fig 3b)** show a striking similarity with this overall-connectivity trend.

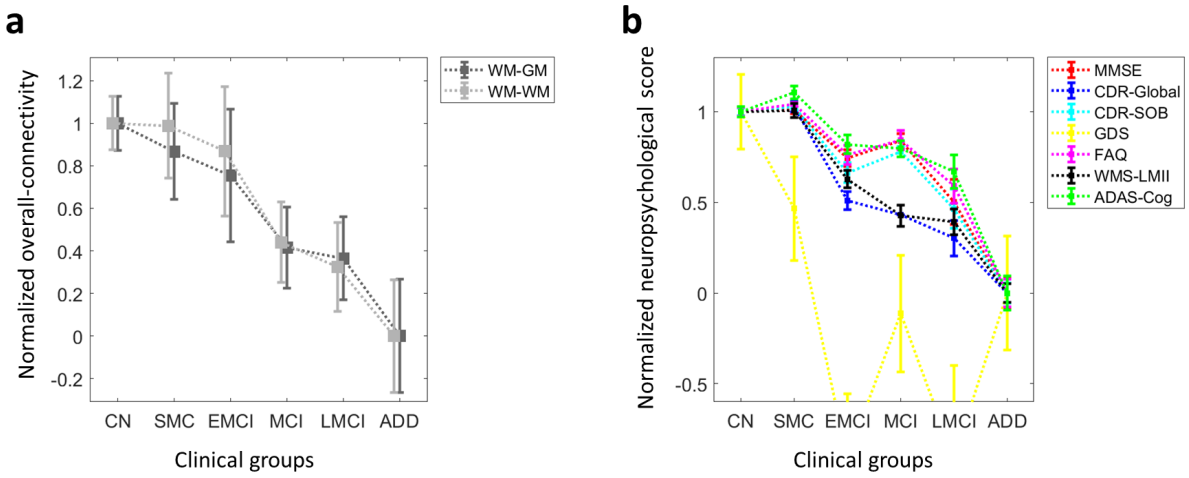

Fig 3. Normalized overall-connectivity and neuropsychological scores for each clinical group in AD progression. (**a**) Normalized group mean (gray square) and standard deviation of mean (gray bar) of the overall-connectivity for each clinical group. The six clinical groups are CN, SMC, EMCI, MCI, LMCI and ADD groups. (**b**) Normalized mean (colored square) and standard deviation (colored bar) of the neuropsychological scores for each clinical group.

Fig 4a-d shows correlation coefficients between elements in FCM_{WW} or FCM_{WG} and neuropsychological scores

which are significantly different from zero (P_{FDR}<0.05). No significant correlations were found between any element in FCM and the Hachinski scale or GDS score.

FCM_{WG} and FCM_{WW} elements within SS_{lr}, CGG_{lr}, CGH_{l}, FXC_{lr}, SCC, PTR_{lr}, and bilateral cerebral spinal tract (CST_{lr}) showed significant positive associations with MMSE scores [34] (**Fig 4a-d**), indicating reduced WM FC corresponds to more severe cognitive impairment. A previous ADNI study found that MMSE scores were strongly associated with a DTI index [35] in SS_{lr}, CGG_{l}, CGH_{lr}, FXC, and SCC. Another study demonstrated WM micro-structural damage was correlated with MMSE, most strongly in temporal lobe [36] where the CGH, FXC and part of SS reside. On the other hand, the lower WM functional connectivity might be also due to damage to GM regions to which the WM tracts connect, including cellular pathology [4] and gross atrophy [37]. GM loss was reported to be strongly correlated with decreases in MMSE in all regions that showed prominent GM atrophy in AD [38].

The CDR-global [39] and CDR-SOB scores are indicators of dementia severity [40]. The sum of negative correlations along WM tracts between FCM and CDR-global was strong in SS_{lr}, CGG_{lr}, FXC_{lr}, SLF_{r}, SCC, GCC, FX, PCR_{lr}, PTR_{lr}, $ALIC_{l}$, and CST_{lr} (**Fig 4a-d**). For the linkage between FCM elements and CDR-SOB score, clear negative correlations were found in SS_{lr}, CGG_{lr}, FXC_{l}, PTR_{lr}, PCR_{lr}, GCC, SCC, $ALIC_{l}$, $RLIC_{l}$, and CST_{r}. A previous study found that diffusivity measures were strongly associated with CDR-SOB in SS_{lr}, CCG_{l}, FXC_{l}, PTR_{l}, PCR_{l} and the entire CC [35].

Negative correlations were dominant in SS_{lr}, CGG_{lr}, PTR_{lr}, PCR_{lr}, SLF_{r}, $ALIC_{l}$, $PLIC_{l}$, GCC and SCC between FCM and FAQ [41] that describe the level of performance of daily function activities (**Fig 4a-d**).

CGG_{lr} showed the most significant negative correlations between FCM_{WG} and the ADAS-Cog [42] score, the overall degree of cognitive decline (**Fig 4a-d**). GCC, SCC, FX, PTR_{lr}, PCR_{l}, CGG_{l}, SS_{l}, showed significant correlation between FCM_{WW} and ADAS-Cog (**Fig 4cd**). A previous study found that diffusivity measures were strongly correlated with ADAS-Cog in GCC, SCC, FXC_{l}, PTR_{lr}, CGG_{l}, and SS_{lr}, among others [35].

SCC, GCC, SS_{lr}, $ALIC_{l}$, PTR_{r}, and CGG_{l} showed stronger positive correlations between FC and the WMS-LMII [43] score, a measure of episodic memory (**Fig 4a-d**). CGG and CGH constitute the major pathways between the hippocampal regions and posterior cingulate cortex (PPC). The intrinsic FC between hippocampus and PPC has been reported to be closely associated with WMS-LM scores in elderly people [44]. A portion of SS connects to temporal lobe and prefrontal cortex which are also engaged in episodic memory processing [45]. Moreover, WM tracts in left hemisphere appear to correlate with WMS-LMII scores more widely and strongly (**Fig 4a-d**), consistent

with previous findings that verbal memory tasks are more sensitive to left hemisphere dysfunction [46] and damage to left temporal lobe has consistently been associated with an impairment of verbal memory [47].

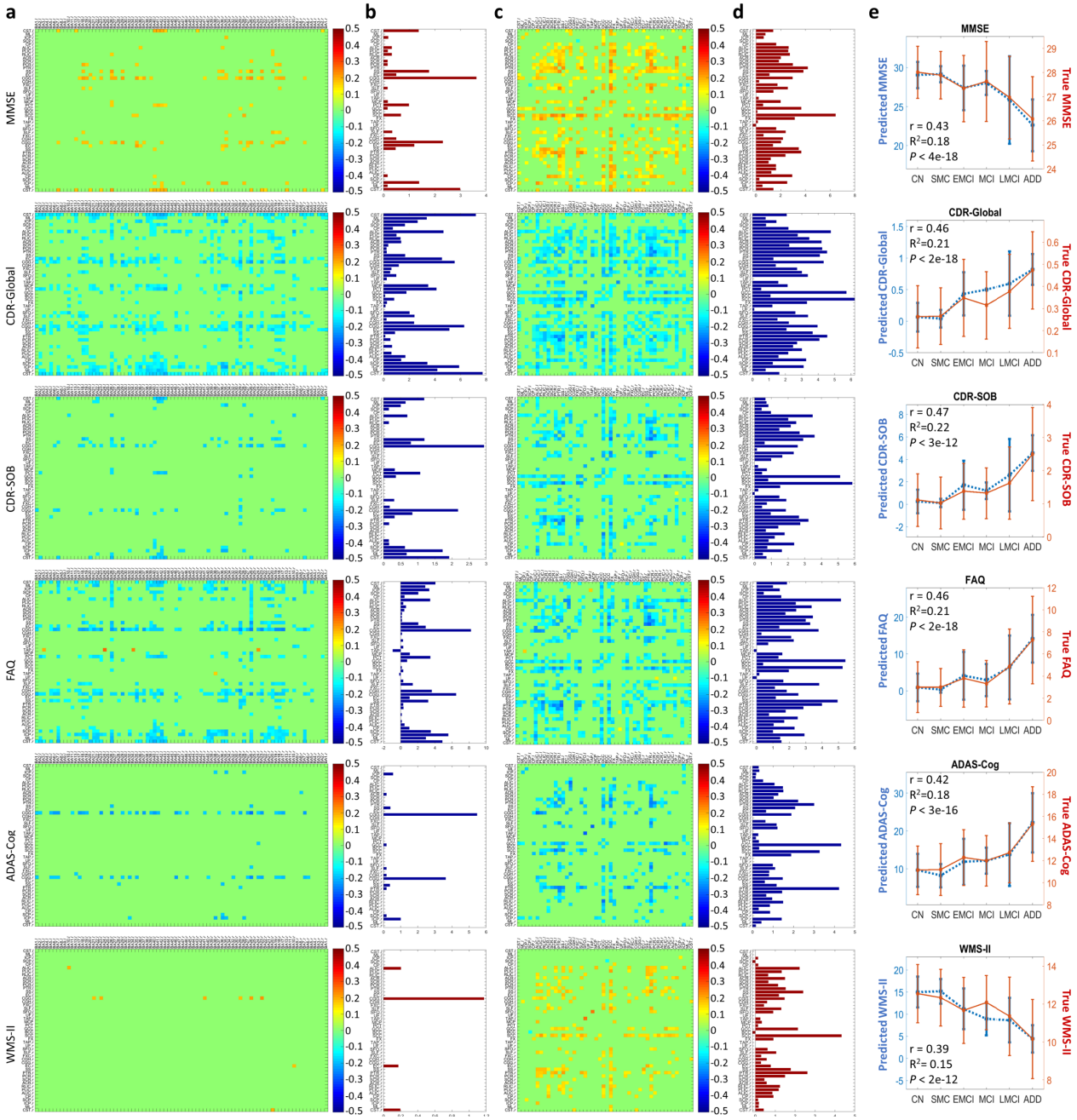

Fig 4. Correlations between WM functional connectivity and neuropsychological scores across all subjects. (**a or c**) Matrix of Pearson's correlation coefficients between single elements in FCM_{WG} or FCM_{WW} and MMSE score, CDR-Global score, CDR-SOB score, FAQ score, ADAS-Cog score, or WMS-LMII score. Each correlation coefficient with $P_{FDR} > 0.05$ was set to be zero. (**b** or **d**) Sum of significant correlation coefficients along each WM tract in **a** or **c**. See **Table 1** for the lists of WM and GM ROIs. (**e**) Group

means and standard deviations of true scores and predicted scores using RF regression model with all WM functional connectivity as initial features. The r, R^2 and *P* in each plot are the Pearson's correlation coefficient between true scores and predicted scores across all subjects, R-square value and *P*-value, respectively.

Correlation between combined WM functional connectivities and neuropsychological scores

The correlation coefficients between the true and RF-predicted scores of ADAS-Cog, CDR-Global, CDR-SOB, FAQ and MMSE were 0.39-0.47 with highly significant *P*-value (<0.001) (**Fig 4e**). The R^2 values in **Fig 4e** indicate that 15%-22% of the variances of those individual scores could be explained by the variance of the overall combined WM functional connectivities, and vice versa.

Prediction of AD stages

The performance of the SVM classification using WM FC features was best for distinguishing ADD from CN group with sensitivity of 0.83 and specificity of 0.81 (AUC=0.87). The performance using optimized features reduced monotonically with addition of patients from earlier stages to the ADD group (**Fig 5**). Also, feature selection helped to improve performance in all the classifications.

a

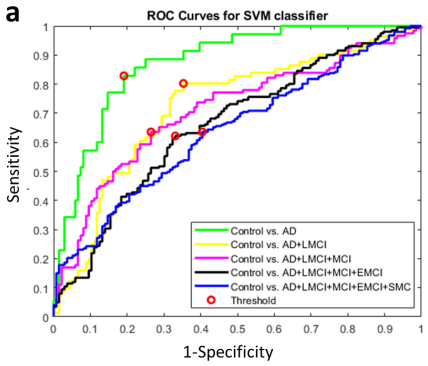

b

	10-fold CV error		ROC Analysis		
	All Features	Optimized Features	Area Under Curve (AUC)	Sensitivity	Specificity
CN vs ADD	29.88	18.12	0.87	0.83	0.81
CN vs ADD+LMCI	34.90	27.52	0.72	0.80	0.65
CN vs ADD+LMCI+MCI	39.68	32.80	0.71	0.64	0.74
CN vs ADD+LMCI+MCI+EMCI	44.61	37.47	0.66	0.62	0.67
CN vs ADD+LMCI+MCI+EMCI+SMC	42.41	38.56	0.64	0.64	0.60

Fig 5. **ROC curves of SVM classifications and a summary of their CV errors, AUC, sensitivity and specificity.** (**a**) ROC curves of SVM algorithm for distinguishing patients from CN. Difference color represents different cumulative group of patients. (b) The errors of 10-fold CV and ROC related indices-AUC, sensitivity and specificity for the classifications.

Discussion

In conventional rsfMRI studies, correlations in BOLD signals between GM regions are interpreted as revealing FC. Extending this concept, we investigated the FC between WM and GM regions or between WM regions for 383 ADNI participants from six subject groups. We mainly found that: 1) LMCI and ADD have significant deficits in

regional WM FC relative to CN, 2) regional WM FC is significantly associated with neuropsychological scores (i.e., MMSE, CDR, FAQ, ADAS-Cog and WMS-LMII), and 3) WM FC can be used to distinguish between patients and controls. To the best of our knowledge, this is the first investigation of novel measures of functional connectivity and degeneration in WM throughout the evolution of AD pathology. Our findings indicate that FC of WM from MRI may serve as a novel in vivo biomarker to identify changes in brain in AD.

In our analyses, we constrained ROIs to GM or WM only in order to avoid partial volume averaging effects which potentially could overestimate the correlation of time-courses between regions. These correlations of WM with GM or other WM volumes are unlikely caused by drainage effects from adjacent GM because cortical drainage occurs outwards, towards the brain surface while deeper WM veins drain inwards to sub-ependymal veins near the lateral ventricles, so there is no direct vascular communication between them [48]. In our analyses we did not regress out global signals because there is growing evidence that they may contain valuable information [49, 50]. Other physiological noises (such as that caused by variations in heart rate and respiration) were, however, regressed out. With these factors in mind, we believe that the WM FC we measured is neither noise effect nor simply a reflection of GM changes.

From a pathophysiological perspective, the decreases in WM FC metrics observed in late AD stages may be directly attributable to GM abnormalities, WM degeneration, metabolic changes and/or cerebrovascular changes. GM abnormalities in AD include the appearance of neurofibrillary/senile plaques, neuronal loss, cell shrinkage, reduced dendritic density and synaptic losses [51, 52]. The consequent neural dysfunction could lead to less engagement of WM in transmission of neural information. WM degeneration during AD progression [53-55] includes demyelination [56] and axonal damage [57], which may also weaken the ability of WM to transfer neural signals between regions. WM degeneration has been reported as a direct consequence of amyloid deposition and tau phosphorylation in GM, and of damage to oligodendrocytes, possibly initiated by ischemia, excitotoxicity, oxidative stress and/or iron overload [58]. Cerebral hypometabolism is found in MCI and AD patients throughout limbic structures, involving hippocampal complex, medial thalamus, mammillary bodies and posterior cingulate. AD patients may also have hypometabolism in amygdala, temporoparietal and frontal association cortex [59, 60]. Cerebral hypoperfusion defects in AD are severe [61], and atherosclerosis that leads to cerebral hypoperfusion is significantly correlated with AD severity. Both hypometabolism and hypoperfusion may have direct effects on BOLD signals in GM and WM. Further studies to understand the relationship between the GM changes and

decreases in WM connectivity in AD are clearly needed and may reflect a combination of factors including direct causes and effects, comorbidities and mutual dependences.

The performances of our SVM classifications indicate that it is feasible to differentiate between CN and AD patients objectively using WM connectivity metrics only. The performance decreases as patients at earlier stages of AD are included sequentially, because there are smaller reductions in WM connectivity early in the disease. The decrease in classification errors using an optimal feature set emphasizes the importance of removing redundant features in the analysis i.e. those WM connectivities that do not contribute new information for the classification. It will be interesting to study in future those specific WM tracts that provide complementary information for maximal differentiation between groups.

Conclusions

The present study indicates that WM functional connectivities 1) decline regionally in LMCI and ADD groups relative to a CN group, 2) are significantly related to cognitive scores, and 3) can serve as machine learning features for distinguishing between AD patients and CN with an acceptable sensitivity and specificity. These findings suggest the potential of WM FC, which has been largely overlooked to date, as a novel neuroimaging biomarker to assess AD progression.

Acknowledgments

The project is supported by the NIH grant R01 NS093669 and a Vanderbilt University Discovery Grant 600670. We also thank the Vanderbilt Advanced Computing Center for Research and Education (ACCRE) for the support of cluster computation.

Data collection and sharing for this project was funded by the ADNI (NIH Grant U01 AG024904) and DOD ADNI (DOD award number W81XWH-12-2-0012). ADNI is funded by the National Institute on Aging, the National Institute of Biomedical Imaging and Bioengineering, and through generous contributions from the following: AbbVie, Alzheimer's Association; Alzheimer's Drug Discovery Foundation; Araclon Biotech; BioClinica, Inc.; Biogen; Bristol-Myers Squibb Company; CereSpir, Inc.; Cogstate; Eisai Inc.; Elan Pharmaceuticals, Inc.; Eli Lilly and Company; EuroImmun; F. Hoffmann-La Roche Ltd and its affiliated company Genentech, Inc.; Fujirebio; GE Healthcare; IXICO Ltd.; Janssen Alzheimer Immunotherapy Research & Development, LLC.; Johnson & Johnson Pharmaceutical Research & Development LLC.; Lumosity; Lundbeck; Merck & Co., Inc.; Meso

Scale Diagnostics, LLC.; NeuroRx Research; Neurotrack Technologies; Novartis Pharmaceuticals Corporation; Pfizer Inc.; Piramal Imaging; Servier; Takeda Pharmaceutical Company; and Transition Therapeutics. The Canadian Institutes of Health Research is providing funds to support ADNI clinical sites in Canada. Private sector contributions are facilitated by the Foundation for the NIH (www.fnih.org). The grantee organization is the Northern California Institute for Research and Education, and the study is coordinated by the Alzheimer's Therapeutic Research Institute at the University of Southern California. ADNI data are disseminated by the Laboratory for Neuro Imaging at the University of Southern California.

References

1. Francis PT, Palmer AM, Snape M, Wilcock GK. The cholinergic hypothesis of Alzheimer's disease: a review of progress. Journal of Neurology, Neurosurgery & Psychiatry. 1999;66(2):137.
2. McKhann G, Drachman D, Folstein M, Katzman R, Price D, Stadlan EM. Clinical diagnosis of Alzheimer's disease. Neurology. 1984;34(7):939.
3. de la Monte SM. Quantitation of cerebral atrophy in preclinical and end-stage alzheimer's disease. Annals of Neurology. 1989;25(5):450-9. doi: 10.1002/ana.410250506.
4. Braak H, Braak E. Neuropathological stageing of Alzheimer-related changes. Acta Neuropathologica. 1991;82(4):239-59. doi: 10.1007/BF00308809.
5. Behrendt G, Baer K, Buffo A, Curtis MA, Faull RL, Rees MI, et al. Dynamic changes in myelin aberrations and oligodendrocyte generation in chronic amyloidosis in mice and men. Glia. 2012;61(2):273-86. doi: 10.1002/glia.22432.
6. Brun A, Englund E. A white matter disorder in dementia of the Alzheimer type: A pathoanatomical study. Annals of Neurology. 1986;19(3):253-62. doi: 10.1002/ana.410190306.
7. Arvanitakis Z, Capuano AW, Leurgans SE, Bennett DA, Schneider JA. Relation of cerebral vessel disease to Alzheimer's disease dementia and cognitive function in elderly people: a cross-sectional study. The Lancet Neurology. 2016;15(9):934-43. doi: 10.1016/S1474-4422(16)30029-1.
8. Lue L-F, Kuo Y-M, Roher AE, Brachova L, Shen Y, Sue L, et al. Soluble Amyloid β Peptide Concentration as a Predictor of Synaptic Change in Alzheimer's Disease. The American Journal of Pathology. 1999;155(3):853-62. doi: 10.1016/S0002-9440(10)65184-X.
9. Agosta F, Pievani M, Geroldi C, Copetti M, Frisoni GB, Filippi M. Resting state fMRI in Alzheimer's disease: beyond the default mode network. Neurobiology of Aging. 2012;33(8):1564-78. doi: https://doi.org/10.1016/j.neurobiolaging.2011.06.007.
10. Binnewijzend MAA, Schoonheim MM, Sanz-Arigita E, Wink AM, van der Flier WM, Tolboom N, et al. Resting-state fMRI changes in Alzheimer's disease and mild cognitive impairment. Neurobiology of Aging. 2012;33(9):2018-28. doi: https://doi.org/10.1016/j.neurobiolaging.2011.07.003.
11. Dennis EL, Thompson PM. Functional Brain Connectivity Using fMRI in Aging and Alzheimer's Disease. Neuropsychology Review. 2014;24(1):49-62. doi: 10.1007/s11065-014-9249-6.
12. Guo H, Song X, Sun Z, Beyea SD, Zhang J, Zhang Y, et al. White matter fMRI activation induced by processing speed tasks in Alzheimer's disease and healthy aging: Preliminary results of a Canada-China Joint Health Research Initiative Project. Radiological Society of North America; Chicago2013.
13. Song X, Guo H, Sun Z, Beyea SD, Zhang J, Zhang Y, et al. Functional MRI activation of the white matter in Alzheimer's disease - Preliminary Results from a Canada-China Joint Health Research Initiative Project. . International Society for Vascular Behavioural and Cognitive Disorders; Toronto2013.

14. Ding Z, Huang Y, Bailey SK, Gao Y, Cutting LE, Rogers BP, et al. Detection of synchronous brain activity in white matter tracts at rest and under functional loading. Proceedings of the National Academy of Sciences. 2018;115(3):595-600.
15. Gore JC, Li M, Gao Y, Wu T-L, Schilling KG, Huang Y, et al. Functional MRI and resting state connectivity in white matter - a mini-review. Magnetic Resonance Imaging. 2019;63:1-11. doi: https://doi.org/10.1016/j.mri.2019.07.017.
16. Gao Y, Li M, Zu Z, Rogers B, Anderson A, Ding Z, et al. Progressive degeneration of white matter functional connectivity in Alzheimer's Disease. SPIE Medical Imaging; San Diego, California, United States2019.
17. Weiner M. Study population. Alzheimer's Disease Neuroimaging Initiative 3 (ADNI3) Protocol2016.
18. Yan C-G, Wang X-D, Zuo X-N, Zang Y-F. DPABI: Data Processing & Analysis for (Resting-State) Brain Imaging. Neuroinformatics. 2016;14(3):339-51. doi: 10.1007/s12021-016-9299-4.
19. Friston KJ, Williams S, Howard R, Frackowiak RS, Turner R. Movement-related effects in fMRI time-series. Magn Reson Med. 1996;35(3):346-55. Epub 1996/03/01. PubMed PMID: 8699946.
20. Ashburner J. A fast diffeomorphic image registration algorithm. NeuroImage. 2007;38(1):95-113. doi: https://doi.org/10.1016/j.neuroimage.2007.07.007.
21. Ashburner J, Friston KJ. Unified segmentation. NeuroImage. 2005;26(3):839-51. doi: https://doi.org/10.1016/j.neuroimage.2005.02.018.
22. Oishi K, Faria A, Jiang H, Li X, Akhter K, Zhang J, et al. Atlas-based whole brain white matter analysis using large deformation diffeomorphic metric mapping: Application to normal elderly and Alzheimer's disease participants. NeuroImage. 2009;46(2):486-99. doi: https://doi.org/10.1016/j.neuroimage.2009.01.002.
23. Lancaster JL, Woldorff MG, Parsons LM, Liotti M, Freitas CS, Rainey L, et al. Automated Talairach Atlas labels for functional brain mapping. Human Brain Mapping. 2000;10(3):120-31. doi: 10.1002/1097-0193(200007)10:3<120::AID-HBM30>3.0.CO;2-8.
24. Power JD, Barnes KA, Snyder AZ, Schlaggar BL, Petersen SE. Spurious but systematic correlations in functional connectivity MRI networks arise from subject motion. NeuroImage. 2012;59(3):2142-54. Epub 2011/10/14. doi: 10.1016/j.neuroimage.2011.10.018. PubMed PMID: 22019881.
25. Cohen J. Statistical power analysis for the behavioral sciences. 2nd ed. New York1988.
26. Benjamini Y, Hochberg Y. Controlling the False Discovery Rate: A Practical and Powerful Approach to Multiple Testing. Journal of the Royal Statistical Society Series B (Methodological). 1995;57(1):289-300.
27. Sengupta A, Ramaniharan AK, Gupta RK, Agarwal S, Singh A. Glioma Grading Using a Machine-Learning Framework Based on Optimized Features Obtained From T1 Perfusion MRI and Volumes of Tumor Components. Journal of Magnetic Resonance Imaging. 2019;0(0). doi: 10.1002/jmri.26704.
28. Loh W-Y. Regression trees with unbiased variable selection and interaction detection. Statistica Sinica. 2002;12:361-86.
29. Zadrozny B, Langford J, Abe N, editors. Cost-sensitive learning by cost-proportionate example weighting. Third IEEE International Conference on Data Mining; 2003 22-22 Nov. 2003.
30. Mayo CD, Mazerolle EL, Ritchie L, Fisk JD, Gawryluk JR. Longitudinal changes in microstructural white matter metrics in Alzheimer's disease. NeuroImage: Clinical. 2017;13:330-8. doi: https://doi.org/10.1016/j.nicl.2016.12.012.
31. Fellgiebel A, Schermuly I, Gerhard A, Keller I, Albrecht J, Weibrich C, et al. Functional relevant loss of long association fibre tracts integrity in early Alzheimer's disease. Neuropsychologia. 2008;46(6):1698-706. doi: https://doi.org/10.1016/j.neuropsychologia.2007.12.010.
32. Rose SE, McMahon KL, Janke AL, O'Dowd B, de Zubicaray G, Strudwick MW, et al. Diffusion indices on magnetic resonance imaging and neuropsychological performance in amnestic mild cognitive

impairment. J Neurol Neurosurg Psychiatry. 2006;77(10):1122-8. Epub 2006/06/07. doi: 10.1136/jnnp.2005.074336. PubMed PMID: 16754694; PubMed Central PMCID: PMCPMC2077533.
33. Jack CR, Jr., Knopman DS, Jagust WJ, Shaw LM, Aisen PS, Weiner MW, et al. Hypothetical model of dynamic biomarkers of the Alzheimer's pathological cascade. The Lancet Neurology. 2010;9(1):119-28. doi: 10.1016/S1474-4422(09)70299-6. PubMed PMID: 20083042.
34. Folstein MF, Folstein ES, McHugh RP. Mini-mental state. A practical method for grading the cognitive state of patients for the clinician. Journal of Psychiatric Research. 1975;12:189-98.
35. Nir TM, Jahanshad N, Villalon-Reina JE, Toga AW, Jack CR, Weiner MW, et al. Effectiveness of regional DTI measures in distinguishing Alzheimer's disease, MCI, and normal aging. NeuroImage: Clinical. 2013;3:180-95. doi: https://doi.org/10.1016/j.nicl.2013.07.006.
36. Bozzali M, Falini A, Franceschi M, Cercignani M, Zuffi M, Scotti G, et al. White matter damage in Alzheimer's disease assessed in vivo using diffusion tensor magnetic resonance imaging. J Neurol Neurosurg Psychiatry. 2002;72(6):742-6. Epub 2002/05/23. PubMed PMID: 12023417; PubMed Central PMCID: PMCPMC1737921.
37. Janke AL, Zubicaray Gd, Rose SE, Griffin M, Chalk JB, Galloway GJ. 4D deformation modeling of cortical disease progression in Alzheimer's dementia. Magnetic Resonance in Medicine. 2001;46(4):661-6. doi: 10.1002/mrm.1243.
38. Thompson PM, Hayashi KM, de Zubicaray G, Janke AL, Rose SE, Semple J, et al. Dynamics of gray matter loss in Alzheimer's disease. Journal of Neuroscience. 2003;23(3):994-1005. PubMed PMID: WOS:000180865400031.
39. Morris JC. The Clinical Dementia Rating (CDR). Neurology. 1993;43(11):2412.
40. O'Bryant SE, Waring SC, Cullum CM, Hall J, Lacritz L, Massman PJ, et al. Staging dementia using Clinical Dementia Rating Scale Sum of Boxes scores: a Texas Alzheimer's research consortium study. Archives of neurology. 2008;65(8):1091-5. doi: 10.1001/archneur.65.8.1091. PubMed PMID: 18695059.
41. Pfeffer RI, Kurosaki TT, Harrah CH, Jr., Chance JM, Filos S. Measurement of functional activities in older adults in the community. J Gerontol. 1982;37(3):323-9. Epub 1982/05/01. PubMed PMID: 7069156.
42. Rosen WG, Mohs RC, Davis KL. A new rating scale for Alzheimer's disease. Am J Psychiatry. 1984;141(11):1356-64. Epub 1984/11/01. doi: 10.1176/ajp.141.11.1356. PubMed PMID: 6496779.
43. Wechsler D. WMS-R: Wechsler memory scale-revised: manual1987.
44. Wang L, LaViolette P, O'Keefe K, Putcha D, Bakkour A, Van Dijk KRA, et al. Intrinsic connectivity between the hippocampus and posteromedial cortex predicts memory performance in cognitively intact older individuals. NeuroImage. 2010;51(2):910-7. doi: https://doi.org/10.1016/j.neuroimage.2010.02.046.
45. Wheeler ME, Buckner RL. Functional-anatomic correlates of remembering and knowing. Neuroimage. 2004;21(4):1337-49. Epub 2004/03/31. doi: 10.1016/j.neuroimage.2003.11.001. PubMed PMID: 15050559.
46. Lee TMC, Yip JTH, Jones-Gotman M. Memory Deficits after Resection from Left or Right Anterior Temporal Lobe in Humans: A Meta-Analytic Review. Epilepsia. 2002;43(3):283-91. doi: 10.1046/j.1528-1157.2002.09901.x.
47. Pillon B, Bazin B, Deweer B, Ehrle N, Baulac M, Dubois B. Specificity of memory deficits after right or left temporal lobectomy. Cortex. 1999;35(4):561-71. Epub 1999/11/26. PubMed PMID: 10574081.
48. San Millán Ruíz D, Yilmaz H, Gailloud P. Cerebral developmental venous anomalies: Current concepts. Annals of Neurology. 2009;66(3):271-83. doi: 10.1002/ana.21754.
49. Murphy K, Birn RM, Handwerker DA, Jones TB, Bandettini PA. The impact of global signal regression on resting state correlations: Are anti-correlated networks introduced? NeuroImage. 2009;44(3):893-905. doi: https://doi.org/10.1016/j.neuroimage.2008.09.036.

50. Saad ZS, Gotts SJ, Murphy K, Chen G, Jo HJ, Martin A, et al. Trouble at rest: how correlation patterns and group differences become distorted after global signal regression. Brain connectivity. 2012;2(1):25-32. doi: 10.1089/brain.2012.0080. PubMed PMID: 22432927.
51. Uylings HB, de Brabander JM. Neuronal changes in normal human aging and Alzheimer's disease. Brain Cogn. 2002;49(3):268-76. Epub 2002/07/26. PubMed PMID: 12139954.
52. Gómez-Isla T, Hollister R, West H, Mui S, Growdon JH, Petersen RC, et al. Neuronal loss correlates with but exceeds neurofibrillary tangles in Alzheimer's disease. Annals of Neurology. 1997;41(1):17-24. doi: 10.1002/ana.410410106.
53. Lee S, Viqar F, Zimmerman ME, Narkhede A, Tosto G, Benzinger TL, et al. White matter hyperintensities are a core feature of Alzheimer's disease: Evidence from the dominantly inherited Alzheimer network. Ann Neurol. 2016;79(6):929-39. Epub 2016/03/27. doi: 10.1002/ana.24647. PubMed PMID: 27016429; PubMed Central PMCID: PMCPMC4884146.
54. Medina D, DeToledo-Morrell L, Urresta F, Gabrieli JD, Moseley M, Fleischman D, et al. White matter changes in mild cognitive impairment and AD: A diffusion tensor imaging study. Neurobiol Aging. 2006;27(5):663-72. Epub 2005/07/12. doi: 10.1016/j.neurobiolaging.2005.03.026. PubMed PMID: 16005548.
55. Roher AE, Weiss N, Kokjohn TA, Kuo YM, Kalback W, Anthony J, et al. Increased A beta peptides and reduced cholesterol and myelin proteins characterize white matter degeneration in Alzheimer's disease. Biochemistry. 2002;41(37):11080-90. Epub 2002/09/11. PubMed PMID: 12220172.
56. Gouw AA, Seewann A, Vrenken H, van der Flier WM, Rozemuller JM, Barkhof F, et al. Heterogeneity of white matter hyperintensities in Alzheimer's disease: post-mortem quantitative MRI and neuropathology. Brain. 2008;131(Pt 12):3286-98. Epub 2008/10/18. doi: 10.1093/brain/awn265. PubMed PMID: 18927145.
57. Scheltens P, Barkhof F, Leys D, Wolters EC, Ravid R, Kamphorst W. Histopathologic correlates of white matter changes on MRI in Alzheimer's disease and normal aging. Neurology. 1995;45(5):883-8. Epub 1995/05/01. PubMed PMID: 7746401.
58. Nasrabady SE, Rizvi B, Goldman JE, Brickman AM. White matter changes in Alzheimer's disease: a focus on myelin and oligodendrocytes. Acta Neuropathol Commun. 2018;6(1):22. Epub 2018/03/04. doi: 10.1186/s40478-018-0515-3. PubMed PMID: 29499767; PubMed Central PMCID: PMCPMC5834839.
59. Nestor PJ, Fryer TD, Smielewski P, Hodges JR. Limbic hypometabolism in Alzheimer's disease and mild cognitive impairment. Ann Neurol. 2003;54(3):343-51. Epub 2003/09/04. doi: 10.1002/ana.10669. PubMed PMID: 12953266.
60. Minoshima S, Giordani B, Berent S, Frey KA, Foster NL, Kuhl DE. Metabolic reduction in the posterior cingulate cortex in very early Alzheimer's disease. Ann Neurol. 1997;42(1):85-94. Epub 1997/07/01. doi: 10.1002/ana.410420114. PubMed PMID: 9225689.
61. Hofman A, Ott A, Breteler MM, Bots ML, Slooter AJ, van Harskamp F, et al. Atherosclerosis, apolipoprotein E, and prevalence of dementia and Alzheimer's disease in the Rotterdam Study. Lancet. 1997;349(9046):151-4. Epub 1997/01/18. doi: 10.1016/s0140-6736(96)09328-2. PubMed PMID: 9111537.